MECHANICAL ENGINEERING SCIENCE

ISSN:2661-4448(online)
2661-443X(print)
Volume 8 No.1 2026

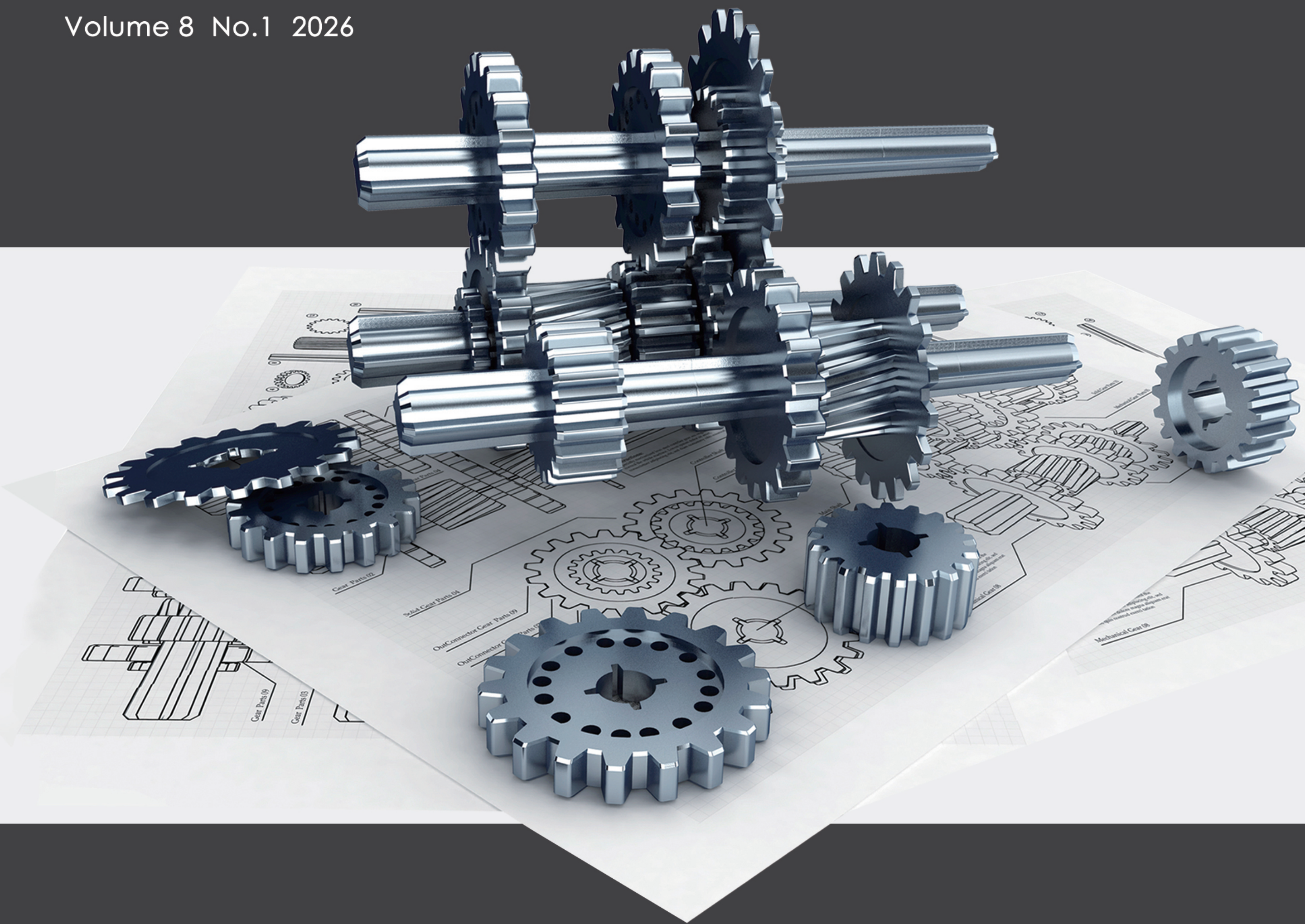

VISER
www.viserdata.com

COMPANY INTRODUCTION

Viser Technology Pte. Ltd. was founded in Singapore with branch offices in both Hebei and Chongqing, China. Viser focuses on publishing scientific and technological journals and books that promote the exchange of scientific and technological findings among the research community and around the globe. Despite being a young company, Viser is actively connecting with well-known universities, research institutes, and indexation database, and has already established a stable collaborative relationship with them. We also have a group of experienced editors and publishing experts who are dedicated to publishing high-quality journal and book contents. We offer the scholars various academic journals covering a variety of subjects and we are committed to reducing the hassles of scholarly publishing. To achieve this goal, we provide scholars with an all-in-one platform that offers solutions to every publishing process that a scholar needs to go through in order to show their latest finding to the world.

Mechanical Engineering Science

VISER

Publisher: Viser Technology Pte. Ltd.

ISSN: 2661-4448(online)

2661-443X(print)

Frequency: Semi-annual

Add.: 195 Pearl's Hill Terrace, #02-41,

Singapore 168976

https://www.viserdata.com/

Mechanical Engineering Science

Volume 8 No.1 (2026)

CONTENTS

Application of Damping Vibration Reduction Technology in Machine Tool Transformation 1

Wenwu ZHANG, Guangchen XU, Lin QIAN

Creative Combination Modeling and Simulation of Planar Linkage Mechanisms Based on SolidWorks 6

Jiaxin SONG, Guangchen XU, Xin JIN, Zhihang XIAO, Xueshu LIU

Simulation Design of Industrial Robot Welding Workstation Based on Robot Studio... 11

Hanyi LI, Guangchen XU, Xin JIN, Jiamin FAN, Xueshu LIU

Design of a Vehicle Mounted Pan Tilt Testing Tamera 17

Zhen YANG

Influence of Bevel Angle on Welding Deformation of X80 Pipeline 21

Peng WU, Liang HAN, Guangchen XU

Design of the New Type Piston Ring Grinding Process 26

Liang HAN, Guangchen XU

VISER

Viser Technology Pte. Ltd.
Mechanical Engineering Science
DOI: 10.33142/mes.v8i1.20089

Research Article Open Access

Application of Damping Vibration Reduction Technology in Machine Tool Transformation

Wenwu ZHANG, Guangchen XU, Lin QIAN*

Yingkou Institute of Technology, Yingkou, Liaoning 115000, China

*__Corresponding Author:__ *Lin QIAN, E-mail: 3141891179@qq.com*

Abstract

The turning tool post is a key structural component of CNC vertical lathes, whose structural characteristics directly determine the machine tool's rigidity, machining accuracy, vibration resistance, cutting efficiency, and service life. Dynamic performance is even the core factor affecting the overall machine performance. Aiming at the cutting chatter problem during the machining of the SXT-032 CNC vertical lathe, this study modified the equipment for damping vibration reduction based on the principle of damping vibration energy dissipation. Measures included optimizing the ram structure of the vertical tool post, adopting a rolling-sliding composite guideway, and integrating a built-in damping system. Practical tests verified that: after modification, under the working conditions of ram extension of 500 mm, cutting depth of 5 mm, and feed rate of 0.5 mm/r, the cutting chatter of the equipment completely disappeared. Machining stability and surface quality were significantly improved, achieving the expected vibration reduction effect.

Keywords: *cutting chatter; CNC vertical machine tool; damping vibration reduction; ram modification*

1 Introduction

In recent years, machining vibration has been extensively studied as a common issue in manufacturing. Among various machining vibrations, self-excited vibration (i.e., cutting chatter)—the most intractable type—is the primary factor restricting high-speed machining stability. Cutting chatter refers to an unstable dynamic process between the machine tool, workpiece, and cutting tool during machining, which is an intense vibration excited by the mechanical system itself. In the machining industry, cutting chatter leads to poor workpiece surface quality, increased machining noise, shortened tool life, and damage to the machine tool system.

The vertical tool post is a critical component of CNC vertical lathes, whose accuracy and performance are closely related to the machine's overall accuracy, reliability, and durability. However, the vertical tool post is also the weakest part in terms of rigidity. Improving its performance—especially vibration resistance—is crucial for enhancing the overall performance of CNC vertical lathes.

2 Problem Analysis of the SXT-032 CNC Vertical Lathe

Figure 1 shows the SXT-032 CNC vertical lathe, with a maximum machining diameter of 6300 mm. The equipment adopts a fixed-beam gantry frame structure (the gantry frame is a purchased welded component), and the vertical tool post uses a T-shaped interface rolling guideway with a maximum vertical stroke of 1000 mm. During machining, the equipment exhibited cutting chatter: the ram and beam slide showed varying degrees of chatter, with the ram chatter being the most obvious. The machined workpiece surface roughness changed significantly, showing chatter textures. Specific phenomena are as follows:

(1) When the ram extension exceeded 300 mm, using a finish turning insert (R 0.4) with a cutting depth of 4 mm and feed rate of 0.5 mm/r, obvious jumping tool marks appeared with significant vibration Figure 2;

Received on February 11, 2026; Accepted on March 15, 2026

(2) When the cutting depth was 1 mm and feed rate was 0.7 mm/r, the effect improved, but the turning trajectory remained obvious and vibration persisted Figure 3;

(3) When the cutting depth was 3 mm and feed rate was 0.3 mm/r, the tool feed was normal; however, when the ram extension reached 500 mm, the ram's cutting performance reached its limit.

Figure 1 SXT-032 CNC Vertical Lathe

Figure 2 Surface Roughness of the Turned Spigot

Figure 3 Cutting Texture of the Turned Workpiece Inner Hole

A test was conducted on the turning plane: when the ram extension reached 650 mm, cutting depth was 2 mm, feed rate was 0.3 mm/r, and worktable speed was 10 r/min, the ram chattered, and slight swing of the ram was visually observable Figure 4.

Figure 4 Turning Texture of the Plane

The authors identified design defects in the equipment as the root cause:

(1) The T-shaped ram of the vertical tool post had an excessively large spacing in the length direction and was an open-type welded structural steel ram. The window opening accounted for 50% of the cavity interface, resulting in severe stiffness loss;

(2) The ram guideway adopted a rolling guideway structure. Although rolling guideways have advantages such as high accuracy, good wear resistance, high sensitivity, and easy maintenance, their poor vibration resistance makes them unsuitable for large-scale turning equipment.

These defects inevitably lead to cutting chatter during machining.

3 Damping Vibration Reduction Modification Measures

3.1 Literature review on chatter suppression

Scholars at home and abroad have conducted extensive research on machining chatter and confirmed that reducing or eliminating tool vibration is key to ensuring machining quality. Relevant studies include:

(1) H Moradia et al. studied the influence of vibration absorber parameters in vibration-damping boring bars on their damping performance and derived corresponding variation laws;

(2) F Bakhtiari et al. designed a dynamic vibration-absorbing boring bar with a large length-diameter ratio and optimized its main parameters;

(3) Suyama et al. used cemented carbide and particle damping rods to improve boring bar rigidity;

(4) Liu Lijia et al. designed a variable stiffness-constrained damping boring bar (composed of a continuous body and a vibration unit) and added an intelligent drive unit at the bar end to realize on-line regulation;

(5) Shen Xingquan et al. developed an adaptive chatter suppression device based on the magnetorheological effect for lathe boring: three piston rod contact blocks (matching the boring bar diameter) were in light radial contact with the boring bar, and built-in magnetorheological fluid moved through the gap between the piston outer wall and cylinder inner wall under piston extrusion to suppress chatter.

3.2 Modification design

This equipment modification drew on the previous

"Research on Dynamic Characteristics of Damping Dynamic Vibration-Reduction Vertical Tool Posts" and took "damping dynamic vibration-reduction tools" as the reference. A "built-in vibration absorber for dynamic vibration-reduction boring bars" was designed for the vertical tool post to improve the chatter stability of the vertical tool post ram. This design is of great significance for enhancing tool post rigidity, solving chatter, improving machining quality and efficiency, and extending tool life.

3.2.1 Ram damping structure modification

The damped dynamic vibration-reduction ram consists of two parts: the tool post ram and the damping system. The damping system includes damping fluid, a vibration-damping block, and annular rubber rings. The damping fluid surrounds the gap between the vibration-damping block and annular rubber rings to provide resistance for the block’s movement. The vibration-damping block acts as the "vibration core" in the ram—according to vibration absorber theory, a heavier mass block enhances damping effect, so the vibration core is made of high-density cemented carbide. The annular rubber rings (installed at both ends of the damping block) serve as supports to prevent contact or elastic collision between the damping block and ram. With a high elastic modulus, the annular rubber rings can provide a certain spring stiffness for the damping block through radial deformation (within the elastic range), showing a linear relationship with the applied load.

During machining, the ram generates cutting chatter under impact loads, and the internal vibration core produces forced vibration. The damping system then absorbs the kinetic energy of the ram vibration to achieve vibration reduction. Specific modifications included:

(1) Sealing the spaced cavities at the bottom of the ram;

(2) Adding 425 steel balls (diameter: 100 mm) and filling the cavities with methyl silicone oil;

(3) Filling the remaining cavities with steel fiber filaments and special micro-expansion grouting material Figure 5.

Figure 5 Structural Modification of the Damping Vibration-Reduction Ram

3.2.2 Guideway upgrade

The guideway was modified to a rolling-sliding composite structure: the original rolling guideway was retained, and a sliding guideway was added. The guideway was wrapped in the vertical tool post slide via side adjustment wedges and upper/lower pressure plates. The moving guideway pair used a 2A12 sliding guideway plate, and the contact surface of the tool post slide was inlaid with Turcite "B" SLYDWAY composite guideway soft belts (produced by SHAMBAN, USA). These soft belts solve long-standing problems of metal-to-metal guideway pairs, as follows:

(1) Anti-crawling performance: According to a report from Loughborough University (UK), the speed-friction coefficient curve of guideway pairs with SHAMBAN soft belts shows a "positive slope". Physicists Burdekin and Bell noted that sliding guideway pairs with a "positive slope" speed-friction coefficient relationship do not experience crawling;

(2) Stable friction coefficient: Tests by Engineer Cognigni (Italy) showed that the friction coefficient of the composite guideway soft belt is 0.05 under dry friction (no lubrication) and 0.03 with lubrication, with stable values;

(3) Excellent wear resistance and accuracy retention: For metal-to-metal guideway pairs, the softer surface

wears more severely (greater hardness difference leads to more wear). The composite guideway soft belt (lower hardness than metal) concentrates wear on itself. Tests showed that under 6 kg/cm ^{2} pressure, the soft belt’s average wear thickness is less than 0.01 mm after 100 km of operation. Under the same working conditions, the accuracy retention of soft belt guideway pairs is 3-5 times that of traditional guideway pairs;

(4) Easy maintenance: When the old metal guideway pair wears, both the ram and vertical slide guideway surfaces need reprocessing. For the modified guideway pair, only the soft belt needs replacement-reducing workload, maintenance costs, and ensuring stable tool post operation and long accuracy retention Figure 6.

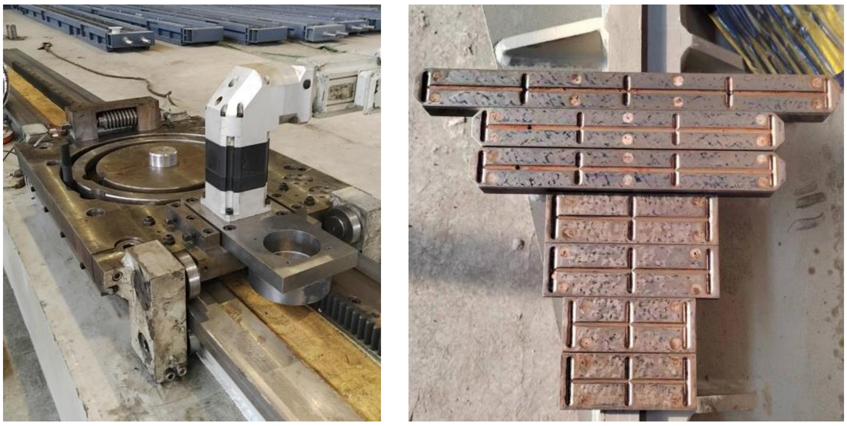

Figure 6 Equipment Modification Process

4 Test Results and Verification

The modification of the SXT-032 equipment was completed in cooperation with Qiqihar Tuoli Metrology Equipment Co., Ltd. Post-modification debugging and damping performance tests were conducted: with the vertical ram extending 500 mm, worktable speed of 12 r/min, intermittent cutting of a typical workpiece’s inner hole (cutting depth: 5 mm, feed rate: 0.5 mm/r), the equipment showed stable machining performance, and cutting chatter completely disappeared Figure 7.

Figure 7 Modified Equipment

5 Conclusions

For the cutting chatter problem of the SXT-032 CNC vertical lathe, this study implemented targeted modifications: optimizing the ram’s damping structure (integrating a built-in damping system with high-density cemented carbide vibration core, steel balls, and methyl silicone oil) and upgrading the guideway to a rolling-sliding composite structure with SHAMBAN Turcite "B" soft belts. Post-modification tests confirmed that the cutting chatter was eliminated under the specified working conditions, and machining stability and surface quality were significantly improved. The modification scheme provides a feasible reference for vibration reduction of large-scale CNC vertical lathes.

Fund Projects: Science and Technology Research Project of Liaoning Provincial Department of Education: Research on the Application of Damping and Vibration Reduction Technology in Key Components of Machine Tools (Grant No. JYTMS20230066).

References

[1] Qin, B. Simulation and Optimization Design of Dynamic Characteristics of Damping Dynamic Vibration-Reduction Boring Bars [D]. Harbin University of Science and Technology, Harbin, China, 2009.

[2] Hou, X.Y.; Ren, X.P.; Ren, C.; Guo, R.F. Structural Design and Dynamic Characteristic Simulation of a Vibration-Reduction

Precision Boring Tool [J]. Chin. J. Mech. Eng., 2019, 21: 78-83. (In Chinese).
[3] Yang, L.Y. Optimization Design and Simulation of Particle Damping and Magnetorheological Composite Vibration-Reduction Boring Tools [D]. North University of China, Taiyuan, China, 2018.
[4] He, M. Dynamic Characteristic Analysis and Optimization Design of Damping Dynamic Vibration-Reduction Tools [D]. Southeast University, Nanjing, China, 2018.
[5] Zhang, W.W.; Xu, G.C.; Qian, L.; et al. Design of High-Precision CNC Vertical Lathe Turning Tool Posts [J]. Mech. Eng. Sci., 2023, 5(1): 22-26.
[6] Shen, X.Q.; Ma, T.; Gao, W.J.; et al. Research on Deep-Hole Cutting Chatter Suppression Devices Based on the Magnetorheological Effect [J]. Tool Eng., 2017, (15): 60-63. (In Chinese)
[7] Zhang, W.W.; Liu, H.; Gao, L.S.; et al. Innovative Design of a New High-Precision Vertical Turning Tool Post [J]. Sci. Wealth, 2022, 14: 314-315. (In Chinese)

Viser Technology Pte. Ltd.
Mechanical Engineering Science
DOI: 10.33142/mes.v8i1.20090

Research Article Open Access

Creative Combination Modeling and Simulation of Planar Linkage Mechanisms Based on SolidWorks

Jiaxin SONG[1], Guangchen XU[1*], Xin JIN[2], Zhihang XIAO[1], Xueshu LIU[3]

1. Yingkou Institute of Technology, Yingkou, Liaoning, 115017, China
2. Dalian Pulandian District Power Supply Company, Dalian, Liaoning, 116200, China
3. Yingkou Hengsheng Machinery Processing Co., Ltd., Yingkou, Liaoning, 115000, China

*****Corresponding Author:** Guangchen XU, E-mail: kanu012@163.com*

Abstract

Planar linkage mechanisms are the most fundamental and widely applied transmission mechanisms in the mechanical field, whose kinematic characteristics directly determine the operational performance of mechanical equipment. Aiming at the poor effect of experimental teaching caused by wear and part loss of physical models in the Mechanical Principle Laboratory of universities, this paper takes the typical planar linkage mechanisms and creative composite mechanisms in the laboratory as the research objects, and conducts research on virtual modeling and motion simulation by using SolidWorks software and its Motion plug-in. Through mapping the dimensions of physical mechanisms in the laboratory, three-dimensional modeling and virtual assembly of eight types of planar linkage mechanisms (including gear-driven double rocker mechanism and crank-rocker double parallelogram composite mechanism) were completed. Kinematic and dynamic data such as angular velocity, angular acceleration and linear velocity of the components were obtained via simulation analysis. The simulation results show that the motion laws of the virtual mechanisms are completely consistent with those of the physical ones, and the variation laws of motion parameters that cannot be observed in physical experiments can be presented quantitatively. This research provides a virtual simulation solution for solving the problem of insufficient mechanical experimental teaching equipment in universities, and also offers a basic method for the design and performance analysis of complex linkage mechanisms.

Key words: *SolidWorks; virtual modeling; motion simulation; planar linkage mechanism*

1 Introduction

Planar linkage mechanisms are extensively used in various mechanical equipment such as engineering machinery, agricultural machinery and light industrial equipment due to their advantages of simple structure, high load-bearing capacity and diverse motion forms. They are the core teaching content of the Mechanical Principle course and also the basic research object of mechanical design. Mechanical Principle Laboratories in universities are usually equipped with physical models of planar linkage mechanisms to intuitively demonstrate the motion laws of the mechanisms. However, physical models are prone to part wear, loss and aging after long-term use, which leads to the failure to accurately achieve the predetermined motion and seriously impairs the effect of experimental teaching. Meanwhile, physical experiments only allow observing the motion state of mechanisms with the naked eye, making it difficult to obtain quantitative parameters such as angular velocity, acceleration and force of components, which cannot meet students' needs for an in-depth understanding of the kinematic and dynamic characteristics of mechanisms.

At present, domestic scholars have applied SolidWorks Motion to the simulation research of rotary tillers, cam-linkage mechanisms and other equipment. Nevertheless, systematic modeling and simulation research on typical planar linkage mechanisms in university laboratories is still scarce, and a complete

Received on February 17, 2026; Accepted on March 24, 2026

simulation system that can directly serve experimental teaching has not yet been formed. Based on this, this paper takes eight types of typical planar linkage mechanisms in the Mechanical Principle Laboratory as the research objects to carry out virtual modeling and simulation research based on SolidWorks. Three-dimensional modeling and assembly are completed by mapping physical dimensions, motion simulation is conducted with the Motion plug-in, and the kinematic and dynamic characteristics of each mechanism are analyzed to verify the consistency between virtual simulation and physical motion. The research aims to provide a virtual simulation scheme for university mechanical experimental teaching, offer a reference for the design, optimization and performance analysis of planar linkage mechanisms, and lay a foundation for the subsequent research of complex composite linkage mechanisms.

2 Basic Theories and Simulation Principles of Planar Linkage Mechanisms

2.1 Composition and classification of planar linkage mechanisms

A planar linkage mechanism is composed of several components connected by lower pairs (revolute pairs and prismatic pairs), with all components moving in the same plane or mutually parallel planes. Its basic components include the frame, driving links, driven links and kinematic pairs. As the most fundamental planar linkage mechanism, the planar four-bar mechanism can be classified into the double crank mechanism, crank-rocker mechanism and double rocker mechanism according to the motion forms of the side links. The judgment of these mechanisms abides by the link length condition: the sum of the lengths of the shortest link and the longest link is less than or equal to the sum of the lengths of the other two links. The kinematic pairs of planar linkage mechanisms are all surface-contact lower pairs, which have the advantages of large load-bearing capacity, slight wear and easy processing and manufacturing. However, their transmission paths are long, which is prone to error accumulation, and the inertial force is difficult to balance, making them unsuitable for high-speed motion [1-4]. In practical applications, a single planar four-bar mechanism can form a composite mechanism through combination and superposition, or be integrated with gears, cams and other mechanisms to meet more complex motion requirements, such as the gear-driven double rocker mechanism and the crank-rocker double parallelogram composite mechanism.

2.2 Calculation of mechanism degree of freedom

The prerequisite for a mechanism to realize a definite motion is that the number of driving links is equal to the degree of freedom of the mechanism. The calculation formula for the degree of freedom of a planar mechanism is as follows:

$$F = 3n - (2P_L + P_H) \tag{1}$$

where n is the number of moving components, P_L is the number of lower pairs, and P_H is the number of higher pairs. In the calculation, the influences of compound hinges, local degrees of freedom and passive constraints must be excluded. Local degrees of freedom have no effect on the overall motion of the mechanism, and passive constraints are redundant constraints; both of them should be eliminated in the calculation to ensure the accuracy of the degree of freedom calculation.

2.3 Simulation principle of solid works motion

SolidWorks Motion is based on the theory of multi-body dynamics and adopts numerical methods to solve the motion equations of mechanisms, which can realize kinematic and dynamic simulation of rigid bodies. Kinematic simulation only considers the motion laws of mechanisms without taking force conditions into account, and can obtain parameters such as displacement, velocity and acceleration of components; dynamic simulation combines factors such as force, torque and inertia to analyze the force and energy consumption characteristics of mechanisms [5-7]. In the simulation process, motion constraints (including motors with constant rotational speed, constant acceleration, etc., and kinematic pairs such as revolute pairs and prismatic pairs) are first added to the mechanism. Then, loads such as gravity, external force and resistance are applied according to actual working conditions. The software solves the dynamic equations, outputs the kinematic and dynamic data of each component, and displays the data intuitively in the form of curves, providing a quantitative basis for the performance analysis of mechanisms.

3 Modeling of Planar Linkage Mechanisms Based on SolidWorks

3.1 Modeling preparation and dimension mapping

Based on the existing physical models of planar linkage mechanisms in the Mechanical Principle Laboratory, calipers, tape measures and other tools are used to map the key dimensions of each mechanism, such as component length, center distance of kinematic pairs, gear module and number of teeth. For mechanisms with inaccurate dimension measurement caused by damage, the dimensions are corrected according to the link length condition and motion laws to ensure that the kinematic characteristics of the modeled mechanism are consistent with those of the physical one. Meanwhile, for mechanisms with gears, standard involute spur cylindrical gears are selected. According to the mapped gear ratio, the module m=2, addendum coefficient h_a^*=1 and clearance coefficient c*=0.25 are adopted, and the reference circle diameter, addendum circle diameter, dedendum circle diameter and center distance of the gears are calculated through gear design formulas [8].

3.2 Three-dimensional modeling and assembly of typical planar linkage mechanisms

Using the Part Design module of SolidWorks, three-dimensional modeling of each component of the mechanisms is completed according to the mapped and calculated dimensions. In the modeling process, the non-critical structures of components are simplified, and the core dimensions affecting the motion of mechanisms are retained. After the completion of part modeling, virtual assembly of each component is realized by adding mating relations (coincidence, concentricity, distance, etc.) in the Assembly module, which accurately restores the connection relations and kinematic pair forms of the mechanisms and ensures that the motion of the assembly is consistent with that of the physical mechanism. In this research, modeling and assembly of eight types of typical planar linkage mechanisms are completed, including the gear-driven double rocker mechanism, crank-rocker double parallelogram composite mechanism, linear motion mechanism, gear swing rod mechanism, oscillating guide bar quick-return mechanism, plow claw telescopic mechanism, crank slider mechanism and double crank mechanism. Their assemblies are shown in Figure 1.

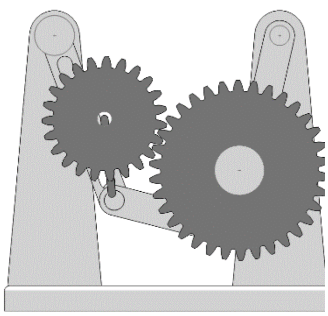

(a) Gear-driven double rocker mechanism

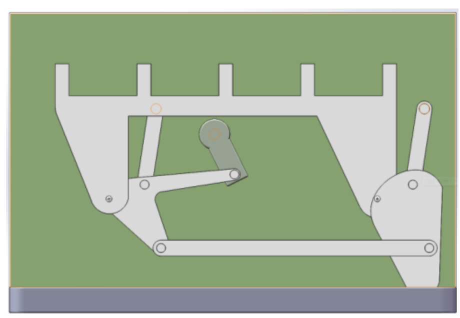

(b) Crank-rocker double parallelogram composite mechanism

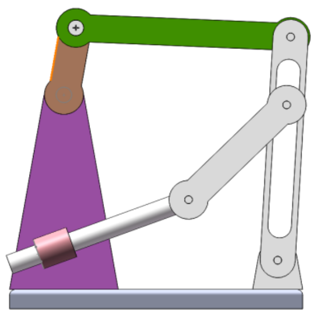

(c) Linear motion mechanism

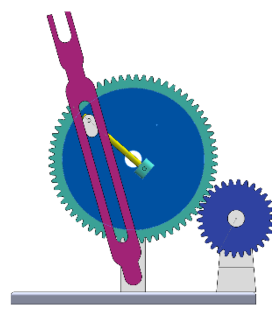

(d) Gear swing rod mechanism

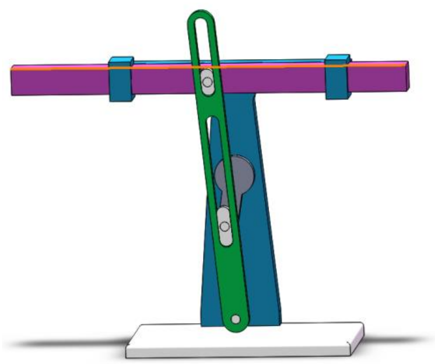

(e) Oscillating guide bar quick-return mechanism

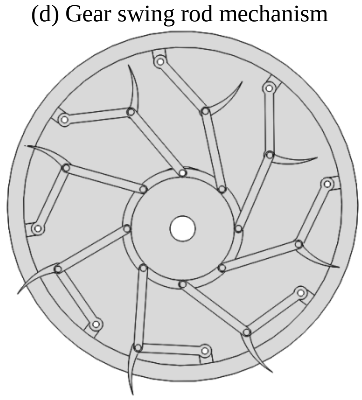

(f) Plow claw mechanism

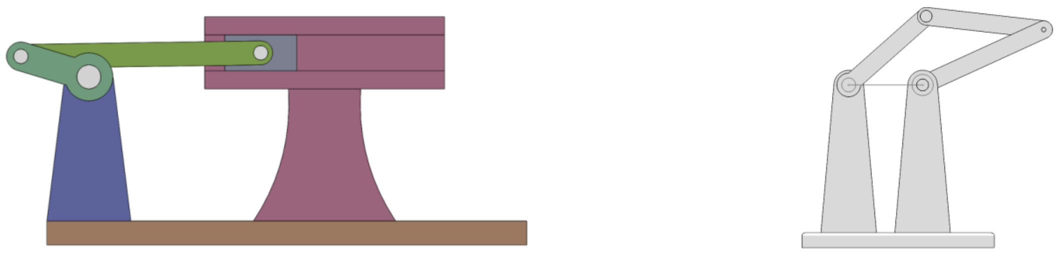

(g) Crank slider mechanism

(h) Double crank mechanism

Figure 1 Assemblies of planar linkage mechanisms

4 Motion Simulation and Result Analysis of Planar Linkage Mechanisms Based on Motion

4.1 Setting of simulation parameters

Simulation parameters are added to the assembly of each mechanism in SolidWorks Motion. The gravity direction is uniformly set to the negative direction of the Y-axis, and a constant-speed rotating motor is added to the driving link according to the actual motion form of the mechanism, with the motor speed set to 5 r/min or 10 r/min. For some mechanisms, a vertical downward external force is applied to the driven link according to working conditions. The simulation time is set to 10~20 s according to the motor speed to ensure that the mechanism completes at least one motion cycle, and the simulation step size is set to 0.01 s to guarantee the accuracy of the simulation results.

4.2 Simulation results and kinematic analysis

After the simulation, data such as angular velocity, angular acceleration, linear velocity, torque and energy consumption of the components of each mechanism are extracted to generate data curves. The motion laws of the mechanisms are analyzed combined with the knowledge of Mechanical Principle and Theoretical Mechanics. The core simulation results and analysis are as follows.

4.2.1 Double crank mechanism

The shortest link of this mechanism serves as the frame, which satisfies the link length condition. A motor with a rotational speed of 5 r/min is applied to the driving link, and its angular velocity is about 30 deg/s with slight fluctuations under the action of gravity. The angular velocity of the long side link of the driven part changes periodically with a period of 12 s, which is consistent with the motor speed, and the maximum angular velocity appears at 10~11 s, as shown in Figure 2.

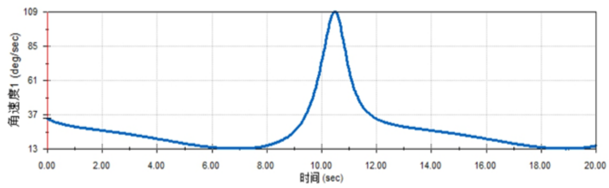

Figure 2 Angular velocity diagram of the double crank mechanism

4.2.2 Crank-rocker double parallelogram composite mechanism

This mechanism is formed by the superposition of a crank-rocker mechanism and a double parallelogram mechanism. A motor with a rotational speed of 10 r/min is added to the driving link, and its angular velocity is about 60 deg/s with the angular acceleration close to 0 during constant-speed rotation. The angular velocity of the driven rocker of the crank-rocker mechanism presents a periodic variation with a steep rise and steep fall trend. In one motion cycle, the angular velocity remains low and stable for most of the time and changes sharply in a short time, which is a typical kinematic characteristic of planar linkage mechanisms, as shown in Figure 3.

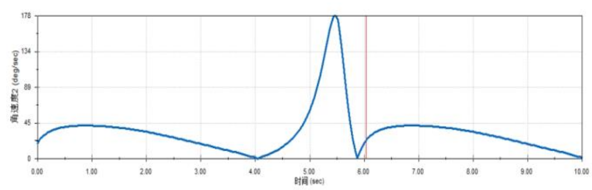

Figure 3 Angular velocity diagram of the crank-rocker double parallelogram composite mechanism

4.2.3 Oscillating guide bar quick-return mechanism

This mechanism has obvious quick-return characteristics. When the driving link rotates at a constant speed, the angular velocity of the guide bar changes periodically at a non-uniform speed, and the maximum angular velocity appears at the position where the driving link is coincident with the axis of the guide bar. The analysis of its motion mechanism shows that the component of the pin velocity on the driving link in the vertical direction of the guide bar is the effective linear velocity of the guide bar, and the closer the pin is to the rotating point on the guide bar, the greater the angular velocity of the guide bar. These two factors jointly result in the quick-return motion of the guide bar, as shown in Figure 4.

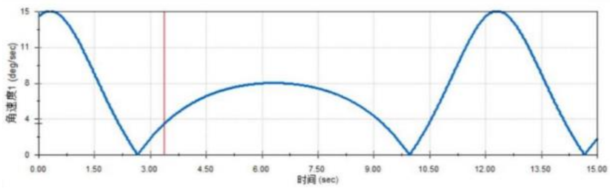

Figure 4 Angular velocity diagram of the oscillating guide bar quick-return mechanism

4.2.4 Crank slider mechanism

When the driving link of the crank slider mechanism rotates at a constant speed, the angular velocity of the connecting rod changes in a sinusoidal function law. The reason is that the component of the linear velocity of the driving link in the vertical direction of the connecting rod is the effective linear velocity of the connecting rod, and this component varies sinusoidally with the rotation of the driving link, as shown in Figure 5.

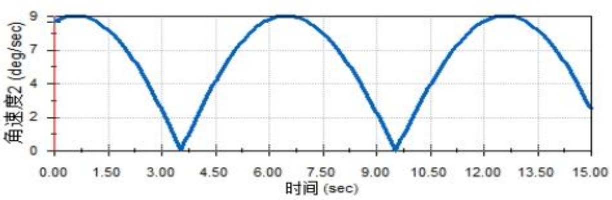

Figure 5 Angular velocity diagram of the crank slider mechanism

5 Conclusions

Taking the planar linkage mechanisms in the Mechanical Principle Laboratory as the research objects, this paper conducts research on virtual modeling, assembly and Motion simulation based on SolidWorks, completes the systematic analysis of eight types of typical mechanisms, and draws the following conclusions:

(1) The SolidWorks three-dimensional model established on the basis of physical mapping dimensions and gear design formulas accurately restores the structural characteristics of the physical mechanism in terms of the connection relations and kinematic pair forms of the assembly. The motion laws of the virtual mechanism are completely consistent with those of the physical one, which verifies the accuracy of virtual modeling.

(2) SolidWorks Motion can accurately obtain quantitative parameters of planar linkage mechanism components, such as angular velocity, angular acceleration, linear velocity, torque and energy consumption. These parameters cannot be observed in physical experiments, which makes up for the deficiencies of physical experiments and provides data support for an in-depth understanding of the kinematic and dynamic characteristics of mechanisms.

(3) The motion parameters of all planar linkage mechanisms change periodically, and there is a strict corresponding relationship between angular velocity, angular acceleration and torque, which is in line with the basic laws of Mechanical Principle and Theoretical Mechanics, verifying the scientificity of simulation results.

Fund Projects: This project was supported by the Yingkou Institute of Technology College Students' Innovation and Entrepreneurship Training Program. Yingkou Institute of Technology campus level research project—Development of food additive supercritical extraction equipment and fluid transmission system research(Grant No.HX202427)

References

[1] Qin S A, Zhou P, Zhou Y J, Jiang H Y. Review on the development status of the belt drive industry [J]. Journal of Mechanical Transmission, 2020, 44(08):1-7.

[2] Pu H Y, Li R C, Huang J G. Dynamic simulation of a rotary tiller based on SolidWorks Motion [J]. Journal of Agricultural Mechanization Research, 2019, 41(06):68-72.

[3] Sun J. Simulation and profile inversion of a cam-linkage mechanism based on SolidWorks Motion [J]. Machinery Design & Manufacture, 2018(05):221-223.

[4] Shang J Z, Zhang Z X. Design of a reconfigurable tracked mobile robot based on a four-bar linkage mechanism [J]. Journal of Mechanical Engineering, 2017, 53(11):123-130.

[5] Zou H J. Mechanical Principle[M]. Beijing: Higher Education Press, 2013.

[6] Shi Y C, Li Z G, Qin S A. Research on meshing dynamics of automotive straight-tooth synchronous belts based on MFBD [J]. Journal of Mechanical Transmission, 2012, 36(09):25-27.

[7] Yu D, Childs T H C, Dalgarno K W. V-ribbed belt design, wear and traction capacity [J]. Proceedings of the Institution of Mechanical Engineers, Part D: Journal of Automobile Engineering, 1998, 212(04):345-356.

[8] Pei C, Vahab M, Sussman M, et al. A hierarchical multiscale model for vibration analysis of complex mechanical systems [J]. Journal of Sound and Vibration, 2000, 233(05):789-806.

Viser Technology Pte. Ltd.
Mechanical Engineering Science
DOI: 10.33142/mes.v8i1.20091

Research Article Open Access

Simulation Design of Industrial Robot Welding Workstation Based on Robot Studio

Hanyi LI[1], Guangchen XU[1*], Xin JIN[2], Jiamin FAN[1], Xueshu LIU[3]

1. Yingkou Institute of Technology, Yingkou, Liaoning, 115017, China
2. Dalian Pulandian District Power Supply Company, Dalian, Liaoning, 116200, China
3. Yingkou Hengsheng Machinery Processing Co., Ltd., Yingkou, Liaoning, 115000, China

[*]***Corresponding Author:*** *Guangchen XU, E-mail: kanu012@163.com*

Abstract

By utilizing the simulation function of Robot Studio software, combined with the graphical programming methods of 3D software UG and ABB Robotics' Robot Studio software, the entire workstation design is completed through steps such as workstation construction, simulation system configuration, I/O configuration, parameter setting, and program writing. This simulation can provide a theoretical basis for the design and path planning of real industrial robot welding workstations, and effectively improve design efficiency.

Key words: *industrial robot; robot studio; simulation*

1 Introduction

Industrial automation requires high efficiency in enterprise production to reduce production costs. It is impractical to spend much time on the inspection or commissioning of industrial robot programming on the production line, as it requires shutdown for teach pendant programming. Offline programming refers to modeling and programming on a computer using software tools without occupying the robot, meaning robot programming operations are performed outside the production line. Offline programming avoids the production "downtime" waste caused by online teach programming. Through robot offline programming, the robot workspace can be better debugged and planned, and design errors can be avoided. During robot programming, offline programming can simultaneously create robot application systems, allowing programming of the robot application system while manufacturing products, thereby enabling early production of products[1].

The industrial robot welding workstation designed in this paper adopts a graphical programming method, which automatically generates the robot's motion trajectory according to the curve characteristics of the 3D model. This method can save time, reduce labor costs, and easily ensure trajectory accuracy. Based on the curve characteristics of the 3D model, the "Auto Path" function of RobotStudio software can be used to automatically generate the running trajectory of robot welding.

2 Construction of Industrial Robot Welding Workstation

The industrial robot welding workstation mainly consists of a robot module, an automobile model, and a welding platform module. The robot module includes an ABB IRB2600 robot and a Binzel water 22 tool. The welding platform mainly imports four completed models into the empty workstation and places them in appropriate positions. The automobile model mainly includes a car body and a car cover model[2].

2.1 Establishment of 3D models

This simulation involves welding the car cover to the car body. Therefore, the car cover and car body

Received on March 5, 2026; Accepted on March 19, 2026

models shown in Figures 1 and 2 are drawn in UG software. The appearance of the model imitates that of an off-road vehicle, with a vehicle length of 575mm, a vehicle wheelbase of 430mm, a maximum vehicle width of 245mm, a maximum vehicle height of 230mm, a distance from the roof to the upper edge of the rear wheel of 120mm, a distance from the hood to the upper edge of the front wheel of 60mm, and a maximum distance of 165mm and a minimum distance of 135mm between the side panels of the vehicle. Since the car cover is to be installed on the car body by welding, welding grooves should be reserved between the car cover and the side panels, with 4mm welding grooves on each side. Therefore, the maximum width of the car cover is 157mm and the minimum width is 127mm. Then, the welding workbench on which the car body and car cover models are placed is imported into the workstation. The welding workbench has a length of 700mm, a width of 600mm, and a height of 400mm. The overall size of the car can be just placed in a suitable position on the workbench.

2.2 Model import and layout

Save the 3D model in SAT format for import into RobotStudio software. Enter RobotStudio software, select "Import Geometry" in the Basic tab, click "Browse Geometry", find the car model just saved on the computer, and import it into RobotStudio software[3]. Due to the inconsistency between the modeling coordinates in UG and the coordinates in the workstation, the position is incorrect during installation and placement. It is necessary to adjust the coordinate axes and set the workpiece coordinates, which usually run in a user-defined Cartesian reference system. Align the X, Y, Z axis directions of the model with those of the workstation to adjust to a direction convenient for installation and placement, as shown in Figure 3 below.

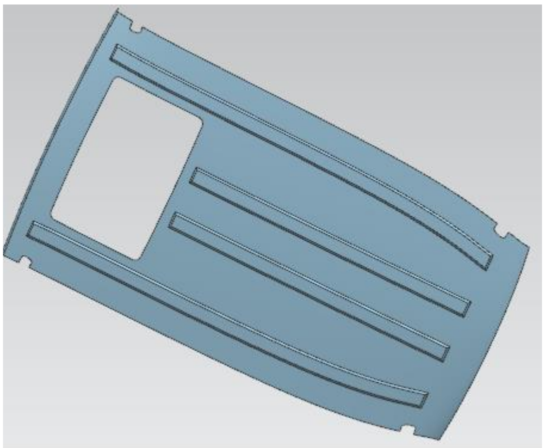

Figure 1 Car cover

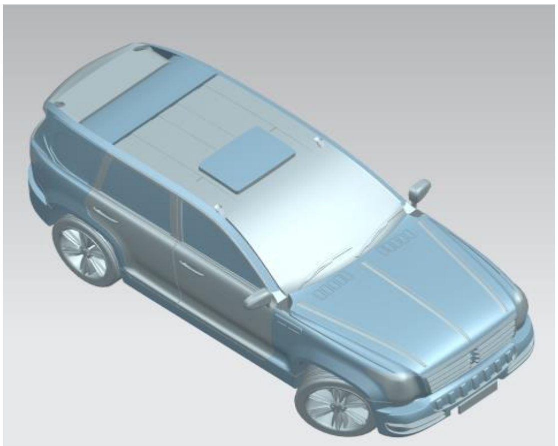

Figure 2 Car body

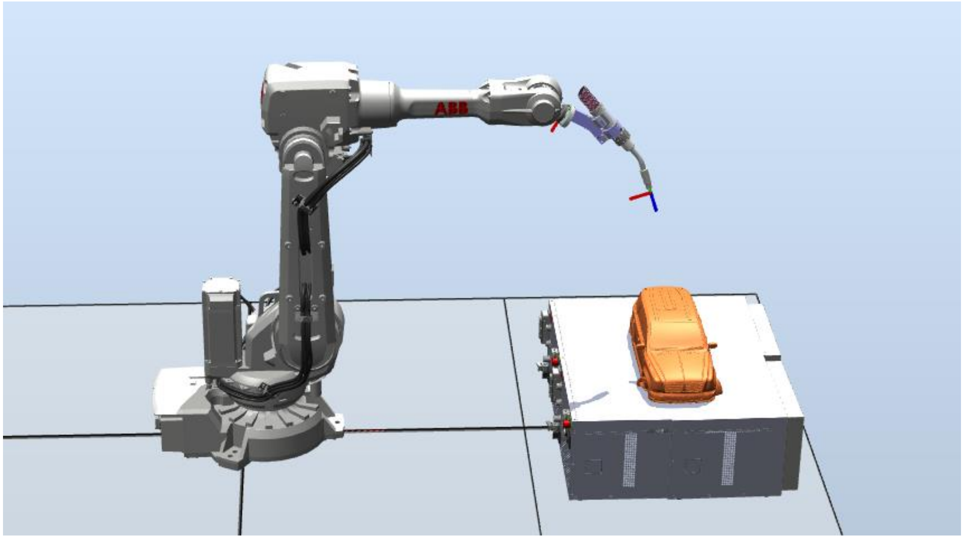

Figure 3 Geometry layout diagram

3 Design of Industrial Robot Welding Simulation System

The design of the industrial robot welding simulation system includes the creation of the robot system, addition of I/O signals, creation and design of Smart components, creation of workstation logic, and writing of welding programs. The design parameters are shown in Table 1 below.

Table 1 Design Parameters

No	Name	Main dimension parameters
1	Welding platform	700×600×400
2	Robot body	IRB 2600_12_165_02
3	Industrial network	709-1 Device net master
4	Bus adapter	840-2 PROFIBUS anybus device
5	I/O configuration	DSQC652 board

3.1 Creation and design of smart components

To realize the welding simulation of industrial robots, it is necessary to truly simulate the welding environment, mainly including the simulation of the light emitted during welding and the weld seam generated by welding. Smart components are efficient tools for realizing animations in RobotStudio. They can realize the animation effect where the light appears during welding, the light disappears when welding is completed, but the weld seam remains on the car model, achieving the restoration of the real environment[4-6].

The creation of Smart components includes the creation of welding laser components and welding seam components. For the creation of welding laser Smart components, two point light sources need to be selected in "Create Light". Change the color to blue to simulate the color of the light, set the diffuse intensity to the highest, set the highlight intensity to the lowest, place the two point light sources at the tip and tail of the welding torch, and then use the Smart components to control the light to appear and disappear during welding.

The creation of welding seam Smart components involves establishing a sphere named "Weld Pool" as the geometry for realizing the weld seam. The length, width, and height of this weld pool should be the same as those of the welding groove. Place the "Weld Pool" in the welding Smart component.

Arrange all Smart components in a suitable position, and finally connect the output signal of the timer with the input signal of the copy. The signal configuration of the welding Smart component is basically completed. The connection of the welding Smart component is shown in Figure 4 below.

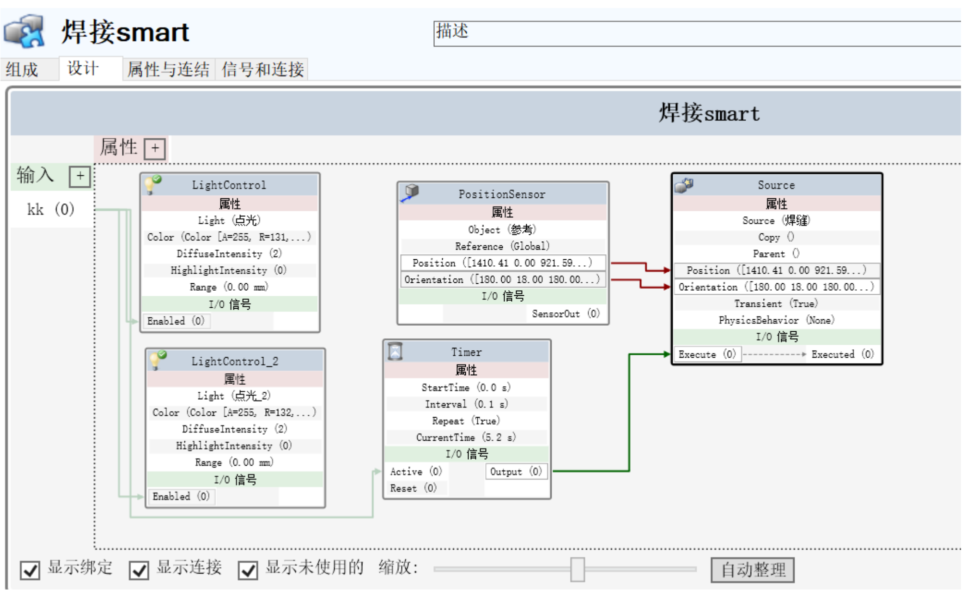

Figure 4 Welding smart component design

3.2 Writing welding programs

Welding programs generally start with ArcLStart or ArcCStart. ArcLStart is usually used as the starting statement, and the welding process generally ends with ArcLEnd or ArcCEnd. The path function is a major feature of offline programming, which visualizes the motion process of the robot tool for user editing. This paper adopts the offline programming method.

When creating a welding path, a red trajectory (i.e., Edge 1) will appear. Change the reference surface to the car cover model. Since the contour of the car cover is not a straight line, arc motion should be performed to make the trajectory more fitting. Therefore, change the approximation parameter to arc motion, and set both the minimum distance and tolerance to 1 to make the trajectory arc more accurate. The created welding path is shown in Figure 5.

4 Industrial Robot Welding Simulation

The industrial robot welding simulation process is shown in Figure 6 below. With the cooperation of the robot's 4 axes, it moves from program point 1 to program point 2, which is the process of the welding torch approaching. Moving from program point 2 to program point 3 is the arc starting preparation stage. During this process, the welding joint will gradually melt under the action of high temperature. The movement from program point 3 to program point 4 is linear, and the movement from program point 4 to program point 5 is arc motion. These two stages are the welding process and arc ending, during which welding trajectories will be formed to realize the connection between the car cover and the car body. From program point 5 to program point 6, no welding is required in this simulation, and no welding trajectory will appear during the simulation. From program point 6 to program point 8, the process from program point 3 to program point 5 is repeated, and finally returns to program point 1, and the program simulation ends.

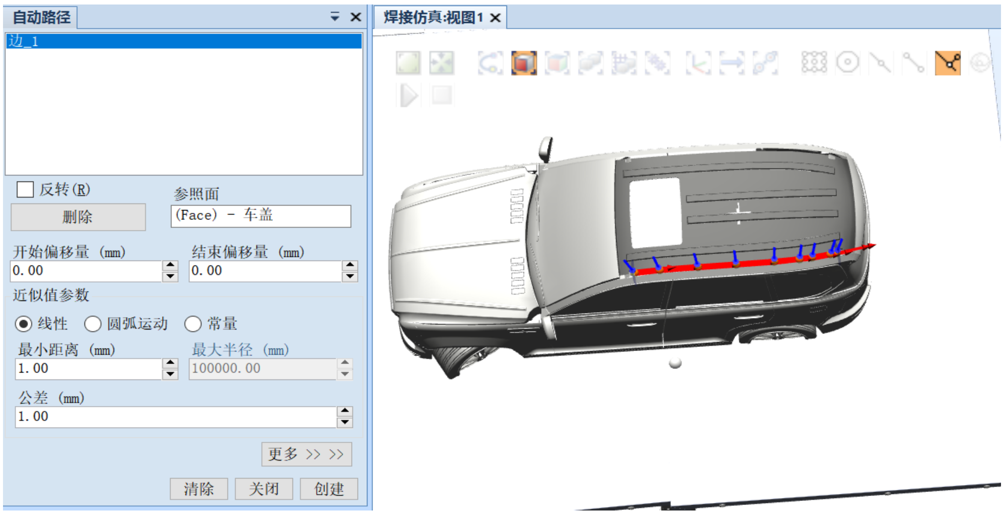

Figure 5 Creation of welding path

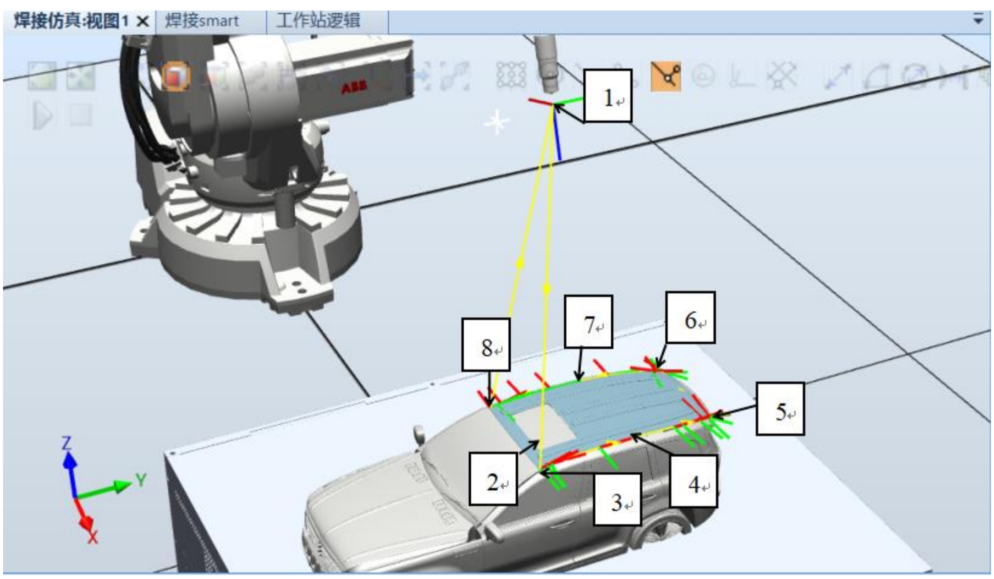

Figure 6 Simulation path design

To be similar to the real welding scene, there should be splashes, sparks, and weld seams during the simulation. The weld seam is formed by geometry movement and copying, and the sparks are replaced by point light sources. The simulation process is shown in Figure 7 below. Figure**7** (a) fills the groove between the car cover and the car body by continuously copying the "Weld Pool" and following the local coordinates of the "Reference" geometry, forming a continuous welding trajectory, i.e., the weld seam. During welding, in addition to the appearance of the weld seam, point light sources emit light to simulate splashing sparks. Figure**7** (b) shows no welding, the point light sources are turned off, and the "Weld Pool" no longer copies with the "Reference" geometry. Figure**7** (c) shows the light and weld seam appearing again, repeating the process of Figure**7** (a).The final welding result is shown in Figure 8.

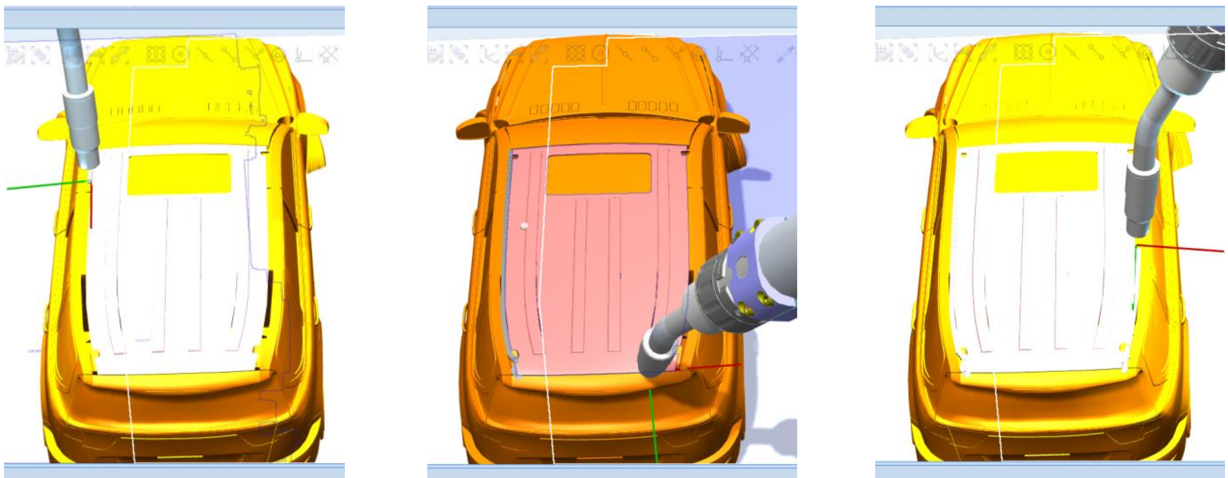

(a) (b) (c)

Figure 7 Welding process diagramt

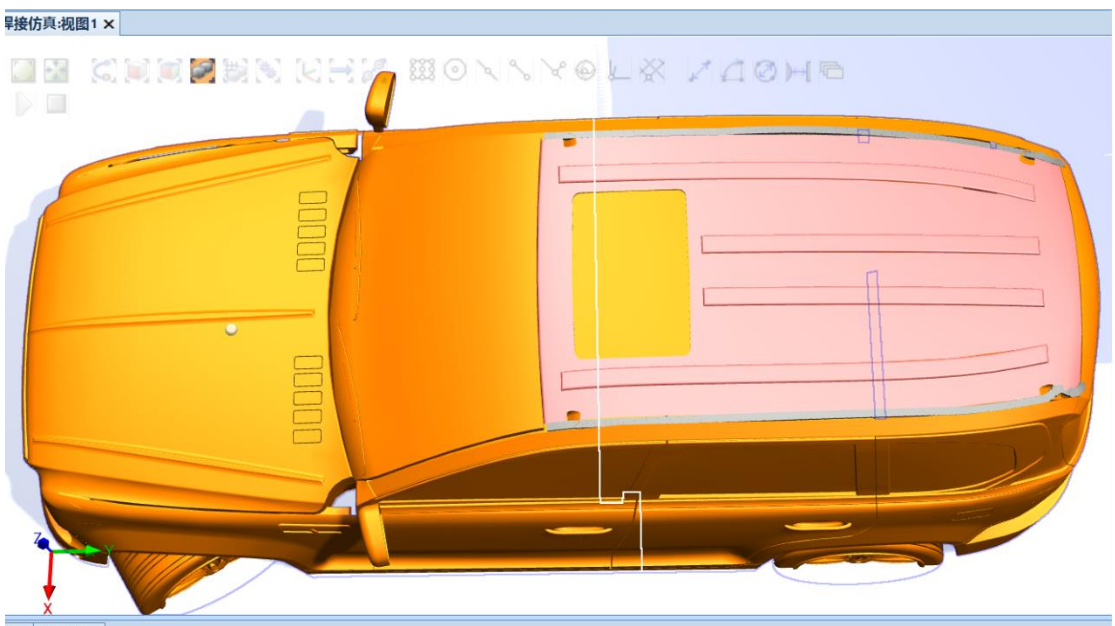

Figure 8 Welding simulation result

From the simulation results, it can be seen that the handling robot and welding robot in the workstation move completely in accordance with the preset sequence and trajectory, completing the handling of the car cover and the welding of the weld seam. All clamping and placing actions of the handling robot, as well as all starting, welding paths, and termination of the welding robot, can meet the preset requirements. The dynamic simulation of the entire process shows the real motion rhythm of the robot, which can illustrate the correctness and applicability of the offline programming simulation program of the industrial robot welding workstation.

5 Conclusion

Starting from the simulated robot welding workstation, this paper presents the structural composition and basic layout of the workstation, and details the process of arc welding workstation system configuration, I/O configuration, parameter setting, program writing, and debugging. The virtual simulation of the workstation runs well and can truly simulate arc welding operations.

Taking the industrial robot welding workstation on the real production line as the research object, this paper uses the graphical programming functions of UG and RobotStudio to design and simulate the path of the robot welding workstation. The design of this welding workstation saves time and labor, easily ensures trajectory accuracy, and reduces the design and commissioning costs of the production line.

Fund Projects: This project was supported by the Yingkou Institute of Technology College Students' Innovation and Entrepreneurship Training Program (Grant: S202514435034) .Yingkou Institute of Technology campus level research project — Development of food additive supercritical extraction equipment and fluid transmission system research(Grant No.HX202427)

References

[1] Zheng Minghui.Simulation Design of Industrial Robot Welding Workstation Based on RobotStudio [J].Modern Information Technology,2020,4(23):118-121.

[2] Ma Junqiang,Guo Chang,CHEN Min. Multi — platform Virtual Simulation Design Based on RobotStudio [J].Electric Drive Automation, 2023,45(05):69-73.

[3] Zhang Xinjuan,Liu Xiangyong,Li Yijing.Simulation Design of Industrial Robot Arc Welding Workstation Based on RobotStudio [J].Mechanical & Electrical Engineering Technology, 2025,54(10):70-74.

[4] Luo Guorong,Qi Jinfeng. Design of Material Sorting Workstation Based on Digital Twin [J].Journal of Beijing Polytechnic College, 2025,24(1):12-17.

[5] Wen Tao, Lin Guixiang , Li Jiecheng, et al. Design and Implementation of a Digital Twin-Driven Desktop Robotic Assembly Line Training System [J]. Mechanical & Electrical Engineering Technology, 2025,54(2):50-53+75.

[6] Lin Hongyu,Lu Xujin. Dising and Virtual Commissioning of Material Sorting Line Base on NX-MCD [J]. Mechanical Engineering & Automation, 2024(6):96-98.

Viser Technology Pte. Ltd.
Mechanical Engineering Science
DOI: 10.33142/mes.v8i1.20092

Research Article Open Access

Design of a Vehicle Mounted Pan Tilt Testing Tamera

Zhen YANG

Yingkou Institute of Technology, Yingkou, Liaoning, 115000, China

**Corresponding Author:* *Zhen YANG, E-mail: 846745608@qq.com*

Abstract

The camera, designed for testing the vehicle-mounted gimbal, boasts compact size, lightweight, and superior imaging quality, enabling more precise debugging of precision gimbals. By optimizing the optical system using ZEMAX optical simulation software and incorporating aspherical elements to improve imaging quality whilereducing the weight of the test camera, the design is manufactured. Finally, the machined aspherical surface is inspected, and imaging quality is verified through image capture.
Key words: *test camera; vehicle mounted pan tilt*

1 Introduction

The vehicle-mounted gimbal is primarily used for outdoor shooting while driving. Since it requires camera imaging, the motion stability of the gimbal is subject to extremely high demands, necessitating the installation of a test camera during factory debugging to evaluate its performance parameters[1]. This test camera must feature excellent imaging quality[2], lightweight design, and minimal impact on the gimbal's movement. Aspherical mirrors can enhance imaging quality[3].

2Optical System Design

2.1 Calculation of initial optical values

Firstly, calculate the entrance pupil diameter D of the camera, as shown in equation (1):

$$D = \frac{f'}{F} \tag{1}$$

In equation (1): D is the diameter of the entrance pupil; f' is the focal length of the lens, taken as 80 mm; F is the F-number of the lens, F=8, and the entrance pupil diameter D is obtained as 10 mm.

According to the field of view, the effective area of the detector can be obtained.

$$\tan\omega = \frac{y'}{f'} \rightarrow 2y' = 2f'\tan\omega \tag{2}$$

In equation (2): ω is the half field angle; If $2y$ 'is the diagonal size of the CCD (charge coupled device) sensor, then the diagonal size of the receiving surface of the CCD sensor of the camera lens can be calculated as $2y'$=39.892mm.

The designed camera is used for vehicle mounted gimbal testing, and the expected parameters of the camera imaging system are shown in Table 1.

Table 1 Camera Design Indicators

parameter	numerical value
MTF (91 lp/mm)	>0.3
CCD receiving surface size（mm）	>39.892
focal length (mm)	80
F#	8
field of view (°)	greater than 28
Object distance（mm）	500 or more to infinity
distortion	<1%
Optical band	visible light band

2.2 Selection of initial structure and correction of aberrations

2.2.1 Selection of initial structure

The selection of the initial optical structure is a prerequisite for the overall design of the optical system. Firstly, it is necessary to meet the basic requirements of lens design in the basic structure

Received on March 24, 2026; Accepted on April 30, 2026

Under the condition of satisfying the requirements, correcting the primary aberration and selecting a suitable initial structure can greatly shorten the design cycle. Select an approximate optical system from existing optical systems by comparing focal length, aperture, and field of view. Choose a double Gaussian optical structure as the initial structure, as shown in Figure 1. The optical system has a total of 25 design parameters, including 12 surface curvatures, 6 lens thicknesses, 5 air gaps, and back focal length.

2.2.2 Correction of aberration

Select the appropriate optical system data from ZEMAX lens design software, and the initial lens design data is shown in Table 2.

Table 2 Initial data of mirror group

	Surface type	curvature radius	thickness	material
object surface		-	infinity	
1	spherical surface	27.057	4.37	HZBAF50_CDGM
2	spherical surface	78.260	0.25	
3	spherical surface	17.975	7.8	HF13_CDGM
4	spherical surface	6.86	1.34	
5	spherical surface	16.93	1.89	HZK6_CDGM
6	spherical surface	11.135	7.13	
7 aperture	spherical surface	-	4.61	
8	spherical surface	-12.84	1.85	HZK20_CDGM
9	spherical surface	-10.84	1.09	
10	spherical surface	-6.91	5.4	F2_CDGM
11	spherical surface	-18.49	0.27	
12	spherical surface	98.2	3.43	HZBAF50_CDGM
13	spherical surface	-10.4	75.6141635	
Imaging surface	spherical surface	-	0	

Using ZEMAX software to simulate an optical system, it was found that there are aberrations in the system that seriously affect imaging quality. Therefore, the parameters of the optical system should be optimized. Optimize the optical system through the default evaluation function in ZEMAX. Additional auxiliary operands are used to balance specific aberrations. The importance of the default optimization function lies in calculating aberrations when the object's light is given from a specific image plane. The default selection is RMS+Spot Radius+Centroid, and then add a small number of custom optimization objectives. Table 3 shows the optimization functions used in the optimization process.

Table 3 Optimization Numbers

Operand	Meaning	Target
EFFL	Effective focal length	8
SPHA	Spherical aberration	0
DIST	Distortion contribution	0
DIMX	Distortion	1%

The following is an analysis of the optimized optical system. The results indicate that there are still aberrations that do not match the initial target. From Figure 1, it can be seen that the value of MTF (modulation transfer function) is much smaller than 0 3@91 lp /mm。 This means that the optical system cannot meet the imaging requirements. Therefore, the system should be optimized more deeply.

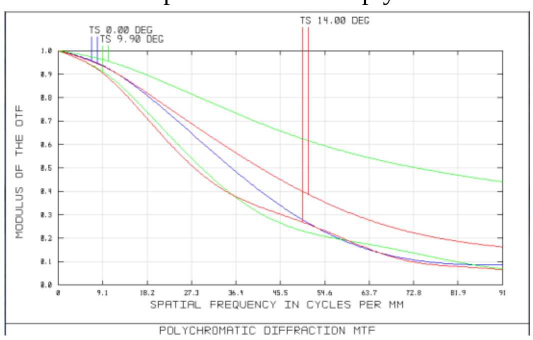

Figure 1 Initial optimized MTF diagram

2.3 Utilizing non spherical surfaces to improve image quality

Non spherical surfaces can be used to correct aberrations and reduce the weight of the lens. Figure 2 shows the effects of correcting spherical aberration using spherical and non spherical surfaces, respectively. In Figure 2, the spherical surface has fewer optimizable factors compared to the non spherical surface, and the non spherical surface has more advantages in correcting spherical aberration.

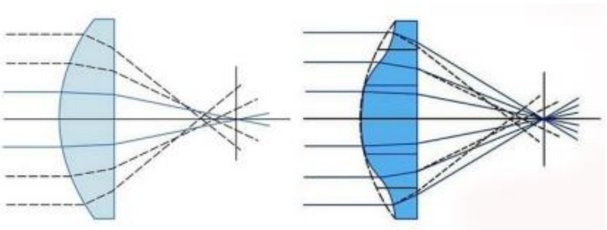

Figure 2 Comparison between spherical and non spherical surfaces

In order to achieve the expected imaging performance, it is necessary to use non spherical surfaces reasonably to correct its primary and higher-order aberrations. Therefore, a surface with a larger ASP is chosen as the non spherical surface. After calculation, select the third surface of the optical system as the non spherical surface. The high-order coefficient data obtained from non spherical optimization are shown in Table 4.

Table 4 High order Non spherical Coefficients

K	a_6	a_8
-1.697116	8.3467e-09	-4.645519e-11

In the simulation of ZEMAX software, a non spherical optical system was established, The radius, thickness, and diameter of each surface are shown in Table 5. Then optimize the optical system by using the previous operands.

MTF curve and as shown in Figure 3. Figure 3 shows that the MTF of all domains is greater than 0.3 @ 91 lp/mm. Compared to the previous MTF curve, the MTF has increased by over 42%.

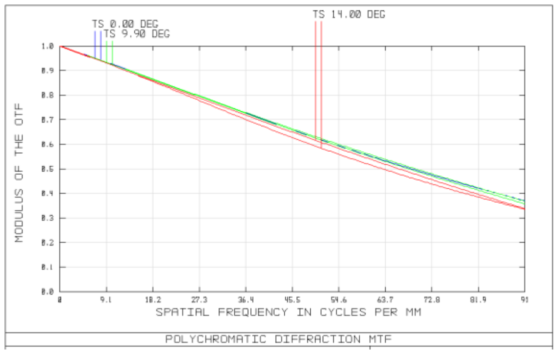

Figure 3 Non spherical optimized MTF diagram

Table 5 Mirror group data

	Surface type	curvature radius	thickness	material
object surface		-	Infinity	
1	spherical surface	18.046	6.4	HZBAF50_CDGM
2	spherical surface	50.12	0.1	
3	Non-spherical surface	34.574	2.4	HF13_CDGM
4	spherical surface	13	5	
5	spherical surface	24.77	2	HZK6_CDGM
6	spherical surface	28.444	2.6	
7 aperture	spherical surface	1e+018	5	
8	spherical surface	-64.993	2.4	HZK20_CDGM
9	spherical surface	-27.427	0.97	
10	spherical surface	-16.218	2.4	F2_CDGM
11	spherical surface	192.31	1.32	
12	spherical surface	402.5	6.2	HZBAF50_CDGM
13	spherical surface	-20.7	62.1258262	
Imaging surface	spherical surface	-	0	

3 Non Spherical Lens Detection Imaging Experimental Testing

3.1 Non spherical lens testing

The actual lens produced after processing is shown in Figure 4. The PV (peak value), Ra (average roughness), and RMS (root mean square) values of the processed non spherical mirror were measured using a ZYGO interferometer, and the final results are shown in Figure 10. The final measured PV is 14 422, Ra is 2 641, RMS is 3.102, both within a reasonable range.

3.2 Imaging experiment detection

Evaluating image quality through resolution is a widely accepted system performance measure. By adjusting the speed control box to adjust the standard resolution drum, the assembled mirror group can obtain the target image. Take a photo of ISO12233 as shown in the figure. Black lines can still be distinguished in the smallest image of the resolution map, meeting the imaging quality requirements of the camera.

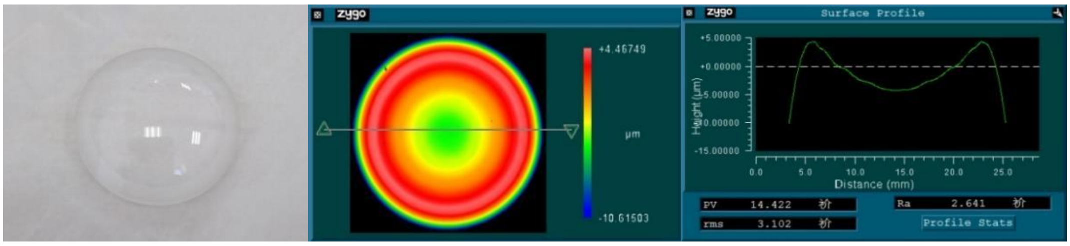

Figure 4 zygo imaging image

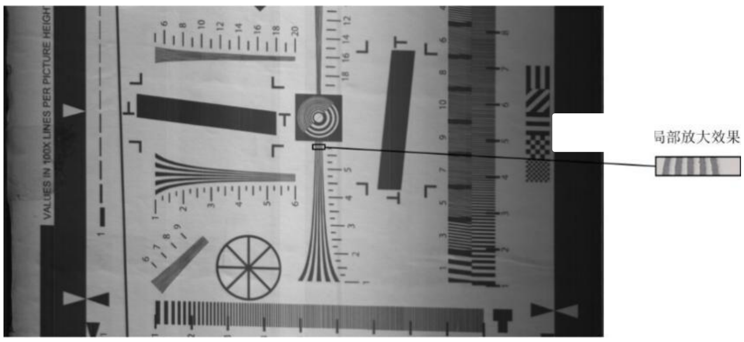

Figure 5 Imaging image of assembled lens

4 Conclusion

Designed and tested a non spherical detection camera. The results indicate that the performance of optical systems based on non spherical surfaces is superior to those based on spherical surfaces. The test proves that the designed vehicle mounted gimbal test camera can meet the design requirements. After optimizing the optical system, the MTF of the optical system is better than 0.3 @ 91 lp/mm. Use ZYGO interferometer to detect the qualification of non spherical mirrors. The test image shows that the camera imaging effect can meet the requirements.

References

[1] Du Kang, Liu Chunyu, Xie Yunqiang, et al. Lens design of micro star sensor with large aperture based on aspheric surface [J]. Chinese Journal of Scientific Instrument, 2019, 40(6): 96-103.

[2] Fan Q P, Wang S Y, Wei L, et al. Uniform long focal depth with centimeter-scale range produced by an aspherical mirror [J]. Optics Communications, 2019, 453: 124342.

[3] Gao F, Jiang Z D, Zhao Z X, et al. Measurement of aspheric surface combining point diffraction interferometry and annular subaperture stitching [J]. Optical Engineering, 2015, 54(1): 014102-014103.

Viser Technology Pte. Ltd.
Mechanical Engineering Science
DOI: 10.33142/mes.v8i1.20093

Research Article Open Access

Influence of Bevel Angle on Welding Deformation of X80 Pipeline

Peng WU, Liang HAN*, Guangchen XU

Yingkou Institute of Technology, Yingkou, Liaoning, 115014, China

****Corresponding Author:** *Liang HAN, E-mail: 312462525@163.com*

Abstract:

X80 steel, renowned for its excellent welding and corrosion resistance properties, is widely used in oil and gas pipeline transportation. During the welding process, the rapid heating at the weld joint and subsequent post-weld cooling generate significant residual stresses and deformations, which severely impact the load-bearing capacity and service life of the welded joint. This study primarily investigates the influence of groove angle on welding deformation by simulating the welding process using Ansys, providing a solid foundation for practical engineering applications.

Keywords: *X80; welding deformation; numerical simulation*

1 Introduction

The petrochemical industry is a pillar local industry in Yingkou City, currently forming two industrial clusters centered around the Yingkou Xianren Island Energy and Chemical Zone and the Yingkou Coastal Industrial Base Chemical Industry Zone. During the industry's development, extensive X80 pipelines have been laid to transport petrochemical products. These pipelines feature a wall thickness of 18.4 mm and a diameter of 1,219 mm, qualifying as large-diameter thick-walled steel pipes. During installation, each pipeline must be welded together. According to welding standards, beveling is required to ensure full penetration depth and complete fusion. This study focuses on analyzing the distribution patterns of welding stress fields under different bevel angles, providing a scientific theoretical basis for optimizing welding processes and reducing residual stresses.

2 Design Concept

In pipeline docking, generally speaking, the larger the bevel angle, the shallower the depth of non fusion, the greater the penetration depth, and the better the welding effect; The smaller the bevel angle, the deeper the depth of non fusion, the smaller the penetration depth, and the more the filling metal accumulates on the surface. However, the angle of the groove should not be too large, as it can cause the bottom of the V-shaped groove to be too thin, and during welding, it is prone to welding defects such as burning through and undercutting due to heat melting. Currently, butt welding of steel pipes requires single-sided welding and double-sided forming, that is, welding on the side of the workpiece with the groove, and the back can also be welded through and form a pattern. This process requirement determines that the current cannot be too small to ensure sufficient filling metal. At the same time, the different groove angles will directly affect the amount of filling metal melt, and the stress generated by the cooling of the molten metal solution will lead to post weld deformation. Therefore, the V-shaped groove welding opening should not be too large, not exceeding 60°. According to the welding manual, the V-groove angle is generally 40°~60° when the plate thickness is 7~26 mm. Similarly, for V-shaped welding, different groove angles can also lead to different deformations. Therefore, this article chooses three schemes of 40°, 45°, and 60° for design comparison.

Received on February 21, 2026; Accepted on March 21, 2026

2.1 Main research methods

A pipe joint with wall thickness of 18.4mm, diameter of 1219 mm, and yield strength of 570 MPa (X80 pipe) is taken as the research object. Using ANSYS finite element software, the thermal-structural coupling method is employed with the birth-and-death unit technique, and considering the nonlinear characteristics of the material under high-temperature conditions, the temperature field, stress field, and deformation of multi-pass welding of the pipe are simulated and calculated. Based on the analysis of the results, an optimized welding scheme for the multi-pass welding of the pipe is obtained.

2.2 Design scheme

Write a program using APDL language of ANSYS software to achieve mobile loading of weld heat source. By using the birth death element method to achieve the movement of heat sources, the nonlinear problems of materials are considered in the finite element analysis of temperature and stress fields. Further simulate and calculate the temperature field, stress field, and deformation of the optimized welding process by changing the groove angle (40°, 45°, 60°, etc.), and compare the results with those before optimization. This provides a scientific theoretical basis for optimizing welding processes and reducing residual stresses.

3 Simulation Process

This study used SOLID 90 for temperature field analysis. This heat source model uses a volumetric heat source. Heat generation rate = $(K \times U \times I) / (A \times V \times DT)$. The welding process uses CO_2 gas protection, and the welding thermal efficiency is lower than that of argon arc welding, so the K value is taken as 0.55. A represents the cross-sectional area of the weld seam, while U, I, and V represent the welding voltage, welding current, and welding speed, respectively (see Table 1 below).

Table 1 Welding Parameters of V - Groove

bevel form	number of plies	current（A）	voltage（V）	Welding speed (mm/s)
V-shaped groove	1	150.00	21.20	3.95
	2	254.00	28.51	4.62
	3	250.00	28.40	5.26
	4	252.00	28.50	6

The formula for the cross-sectional area of the X80 pipeline bevel heat source is as follows:

$$A_1=3.14\times4\times4\div6$$
$$A_2=3.14\times(8\times8-4\times4)\div6$$
$$A_3=3.14\times(12\times12-8\times8)\div12$$
$$A_4=3.14\times(12\times12-8\times8)\div12$$

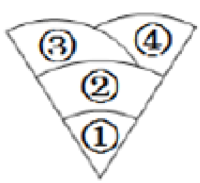

Figure 1 Schematic diagram of V-shaped groove shape

As shown in A1's formula, it represents one-sixth of the area of a circle with a radius of 4. Therefore, we selected two bevel angles of 40° . Both angles are divisible by 360° , making them suitable for heat source calculations. Comparing these three angles effectively demonstrates the deformation distribution patterns. The welding deformation of V-shaped bevels at 40° , and 60° is analyzed.

3.1 Grid division

(1) Select a surface or volume and divide it into tetrahedrons or hexahedrons. Common commands include: esize, amesh, vmesh.

(2) Set the subdivision level or equal divisions for all lines, then perform sweep or free division on the opposite face or volume. Common commands include: vsweep, vemsh.

(3) Create a surface and perform meshing on it. Common commands for stretching it into a meshed volume include: vext.

3.2 Define material properties

The physical properties of metals, including elastic modulus, yield stress, thermal conductivity, and specific heat capacity, vary with temperature. However, many metallic materials lack complete thermophysical parameters, particularly in high-temperature regions where specific heat capacity and thermal conductivity fluctuate with actual plastic deformation. Therefore, these thermophysical parameters must be incorporated into ANSYS analysis.

Table 2 Thermophysical Parameters of X80 Steel

order number	temperature (℃)	Density (kg/m^3)	specific heat capacity (J/(kg・K))	Thermal conductivity (W/(m・K))
1	20	7820-7850	460-470	50-54
2	100	7810	571	52
3	200	7790	660	50
4	400	7720	1084	47.7
5	600	7680	914	38
6	800	7610	1160	27.6

3.3 Loading of life-and-death units

During ANSYS operation, the system does not physically remove "killed" elements from the model. Instead, it applies a minimal factor (default: 1.0E-6) to their stiffness matrices, effectively nullifying load vectors. When elements are "born" (reactivated), they are not newly added but reactivated. The solver cannot generate new elements; to "add" one, it must first deactivate it and reactivate it during a valid load step. Upon reactivation, the element's stiffness, mass, and load values revert to original parameters, while the reactivated element retains no strain history or heat storage.

3.4 Analysis of V type bevel temperature field and stress field

First, we analyze the temperature field and stress field of the plate butt to find the distribution law of the residual stress of the V-shaped groove, and then apply this law to the pipe butt to find the influence of different groove.

The experimental results demonstrate that as the heat source is loaded and moved, the temperature distribution on the butt plate exhibits symmetrical characteristics. Temperature rises more rapidly near the heat source while remaining slower in distant areas, with the plate's outer sections gradually heating up. At step 31, the maximum temperature around the heat source reaches 1651℃, indicating a stable temperature field. As the heat source moves uniformly, the temperature in the weld-free regions of the plate increases from the initial room temperature of 25℃ to 25.05℃.

From Figure 4, it can be seen that the deformation increases as the free end moves farther from the weld zone. From the left side of Figure 5, the stress distribution cross-section of the butt joint, we can observe that the stress is mainly concentrated at the bottom of the weld, i.e., the bottom of the V-shaped opening, showing an increasing trend in the thickness direction.

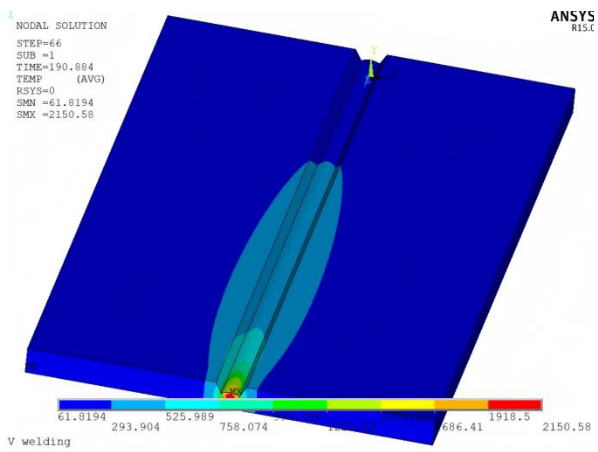

Figure 2 Temperature field at half loading

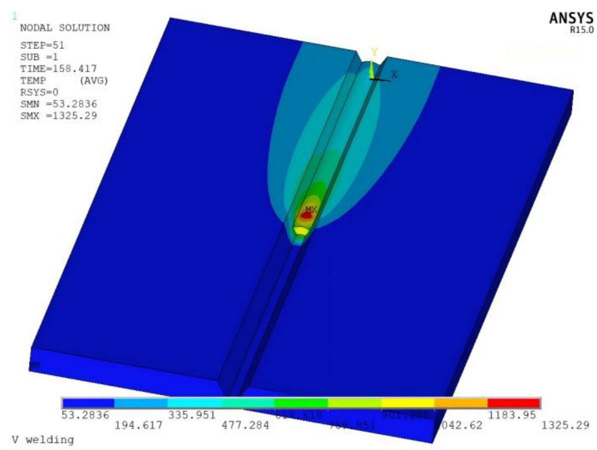

Figure 3 Temperature field after full loading

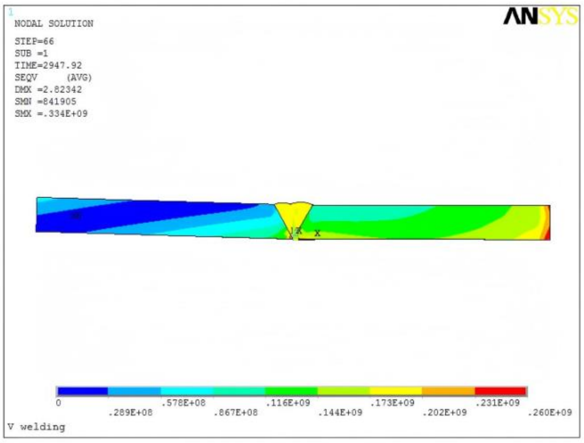

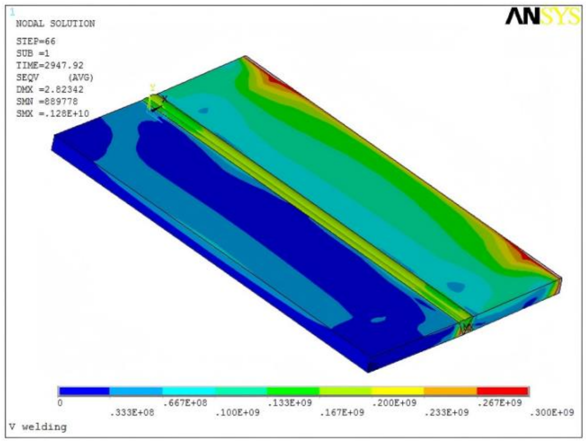

Figure 4 Overall von Mises stress map

Figure 5 Cross-sectional von Mises stress map

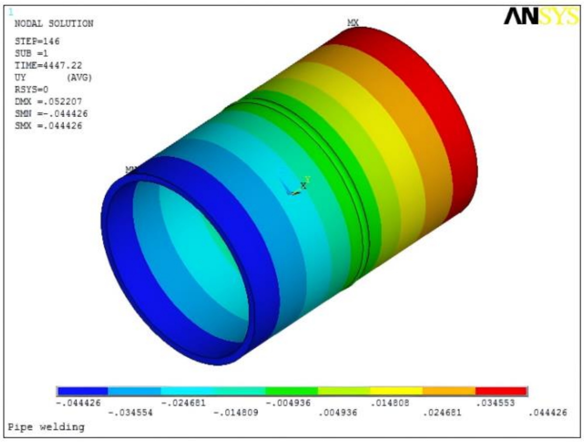

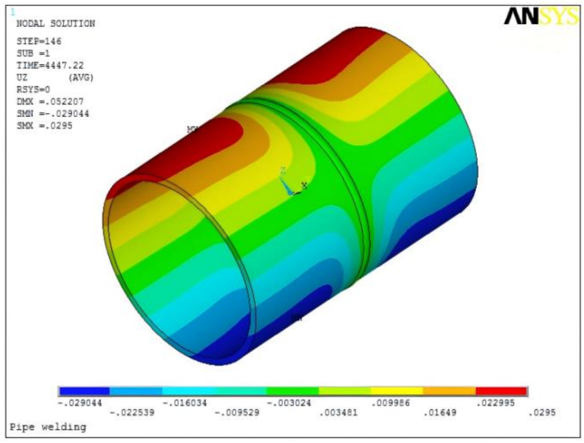

Figure 6 Deformation diagram of 40° bevel

Figure 7 60° bevel deformation diagram

3.5 Simulation of pipe joint deformation for two types of bevel angles

Figure 7 shows that the greater the distance from the weld area to the free end, the more significant the deformation becomes. The overall stress on the upper surface of the welded part is higher than that on the middle and lower surfaces. Post-weld stress is primarily concentrated at the bottom of the weld seam, specifically at the base of the V-shaped opening, with a gradual increase in thickness direction.

The three images demonstrate that the V-groove deformation measures 4.66mm at 40° , and 2.82 mm at 60° , showing a gradual decrease with increasing angle until reaching its minimum at 60° . Therefore, for pipeline butt joints, a 60° V-groove is recommended.

4 Conclusion

This study primarily uses ANSYS software to simulate the temperature field and stress field of X80 pipelines during the welding process. Based on the simulation results, continuous optimization is carried out, providing directions and specific methods. It proves the feasibility of numerical simulation analysis in solving welding problems, which can accurately reflect the distribution patterns of residual stress and deformation. During welding, the temperature field is distributed in a quasi-steady state, with the heat source moving dynamically. The temperature increases more sharply at points on the weldment closer to the heat source. Post-weld stresses are mainly concentrated at the bottom of the weld, specifically at the bottom of the V-shaped opening, showing an increasing trend in the thickness direction. The welding deformation decreases gradually with increasing angle, reaching a minimum value at 60°. As the bevel angle increases, the number of welding layers required increases, the amount of filler metal needed increases, and the grinding becomes more difficult. Therefore, for pipeline butt welding, a 60° bevel should be preferred, which saves processing time and achieves good performance.

Fund Projects: The Foundation of Liaoning Provincial Key Laboratory of Energy Storage and Utilization (CNNK202522).

References

[1] Lu Anli, Cai Zhipeng, Zhao Haiyan. String heat source model and its application in numerical simulation of welding [J]. Journal of Mechanical Engineering, 2001,37(4):26-27.

[2] Dai Qinghua, Ji Peng, Yin Chenbo, et al. Effect of welding sequence on residual stress in butt welding of medium and thick plates [J]. Mechanical Design and Manufacturing, 2011, (7):64-66.

[3] Zhou Guangtao, Liu Xuesong, Yan Dejun, et al. Prediction of reduced welding deformation through optimized roof welding sequence [J]. Journal of Welding, 2009,30(9): 109-112.

[4] Huang XH. Effect of welding residual stress on structural performance[J]. Field Experience, 2011,01(009):67-72.

[5] Sun Yingxue, Sun Ping. Research on Finite Element Analysis Technology for Welding Residual Stress [J]. Nuclear Power Engineering, 2009,2(30):33-35.

[6] Cao Junhui, Huo Lixing, Zhang Yufeng. Finite element analysis of residual stress in low-carbon steel pipe welding [J]. Welding, 2000(12):11-15

[7] Yang QX, Zhao JH. Computer simulation of residual stress field in overlay welding metal [J]. Journal of Welding, 2001,22(3):44-46

[8] Jiang H. Effect of microstructure of Q235 steel welded joint on corrosion resistance of welds [D]. Daqing: Northeast Petroleum University, 2014.7.

Viser Technology Pte. Ltd.
Mechanical Engineering Science
DOI: 10.33142/mes.v8i1.20094

Research Article Open Access

Design of the New Type Piston Ring Grinding Process

Liang HAN, Guangchen XU*

Liaoning Provincial Key Laboratory of Energy Storage and Utilization, Yingkou, Liaoning, 115014, China

***Corresponding Author:** *Guangchen XU,kanu012@163.com*

Abstract:
Among the numerous components of an engine, piston rings are an important part, and their machining quality has a significant impact on the performance of the engine. There are a small amount of burrs on the surface of the piston ring after processing. Traditional deburring equipment, similar to grinding machines, has problems such as high labor intensity and low automation level, which cannot meet the production needs of modern enterprises. This article proposes a new intelligent production line solution that achieves full process automation control based on PLC from feeding to brushing and grinding to final cutting. A dual objective optimization model for grinding energy consumption and time is established, and the optimal process parameters are determined. This design can solve the problem of continuous processing while achieving unmanned and automated processing, avoiding the decrease in accuracy and production efficiency caused by secondary clamping, and improving the profit margin of the enterprise.
Keywords: *piston ring; automated grinding*

1 Objective and Significance

As a metal elastic ring that moves in the axial, radial, and rotational directions inside the engine, the piston ring, when assembled into the ring groove inside the engine cylinder block, will reciprocate together with the piston, providing power support for the engine. High quality piston rings are crucial for engines as they serve multiple functions such as guiding support, ensuring airtightness, and achieving lubrication. In the machining process of piston rings, burrs are inevitably generated on their surfaces. Large and sharp burrs can cause serious particle wear, which can have a slight impact on the service life of the engine. In severe cases, it can lead to engine failure or even damage.

Figure 1 Piston Ring

The six types of burrs shown in Figure 2 are common defects on the machined surface of piston rings. The essence of burrs is the sharp protrusions generated by extrusion on the surface of the piston ring (i.e. the machined surface) after machining due to insufficient selection of machining parameters, machining allowances, and tool types during metal processing. The difficulty of handling burrs varies among different materials. For K1 series materials, due to their low toughness, burrs are easily removed. However, for ductile iron, due to its high toughness, the burrs formed are not easily removed and are very sharp. If we don't remove the burrs before assembling the piston rings into the engine, larger burrs will fall off after installation, causing wear during reciprocating motion and accelerating the damage of the engine piston rings and cylinder liners, resulting in the engine not working properly.

At present, there are various techniques for removing piston ring burrs in the industry, such as ultrasonic deburring, centrifugal grinding, magnetic grinding, etc. However, these methods are relatively expensive, have low processing efficiency, and have a narrow application range. Most companies use single

Received on March 10, 2026; Accepted on March 28, 2026

Serial Number	Burr form	Schematic diagram
1	Sharp burrs on the outer edges and corners	
2	Internal edge burrs	
3	Open end face burrs	
4	Burrs at the opening of the oil tank	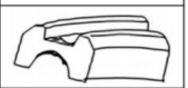
5	Burr on the open end of the ladder surface	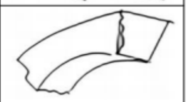
6	Oil hole burrs	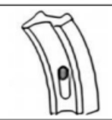

Figure 2 Six forms of piston ring burrs

Figure 3 Physical images of existing external brush equipmen

station brush equipment with a structure similar to an external cylindrical grinder for deburring operations (refer to Figure 3). This device is easy to operate, cost-effective, and has strong adaptability. However, this mode of operation relies heavily on manual loading and unloading, resulting in high labor intensity. Not only is the production pace slow, but there are also differences in manual clamping force, leading to poor product consistency. And due to the single station nature of the machine, which can only be operated by one person, continuous processing is not possible, which consumes a lot of time in process connection and results in low production efficiency. In response to the above issues, an intelligent upgrade design has been carried out this time, introducing robotic arms and automation control technology to replace traditional manual single station operations, and establishing a continuous intelligent production line including material picking, clamping, brushing, grinding, and unloading. This has important engineering application value for eliminating quality hazards and improving the core competitiveness of enterprises.

2 Design Plan

2.1 Design of multi-station seeding tooling

The traditional single-station operating equipment, with only one feeding ring, affects the processing progress. This production line is equipped with three horizontally placed feeding racks, where workers place the piston rings after sorting them. When the production line starts working, it requires circular feeding to ensure that there is always material on the feeding racks to complete the processing process. This realizes an automated processing process of feeding, operating, processing, and collecting materials simultaneously, significantly improving efficiency.

2.2 Design of intelligent production line

This design scheme establishes a fully automated control system based on Siemens PLC, achieving seamless connection from material loading to unloading: processes such as material retrieval by robotic arm → material pushing → clamping → grinding → unloading. The PLC part is designed using the SIEMENSE system, and equipped with industrial vacuum cleaners and hydraulic stations. It includes the following structures:

① Feeding rack *3 (effective length 720mm);
② Material pushing mechanism;
③ Feeding mechanism part;
④ Part of the workstation for clamping;
⑤ Clamp the feeding mechanism part;
⑥ Clamping and rotating mechanism part;
⑦ Brushing and grinding mechanism part;
⑧ Material feeding and grasping mechanism part;
⑨ Lower cooking ring mechanism part.

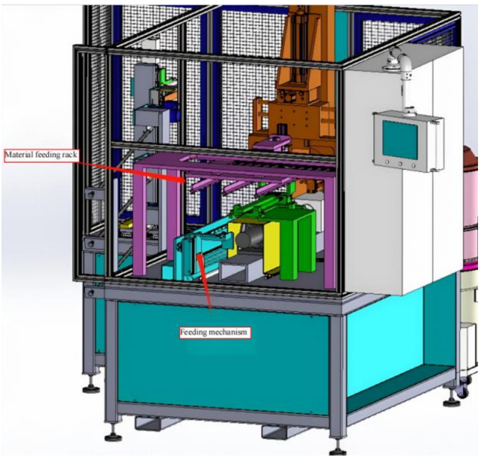

Figure 4 Schematic of the loading rack

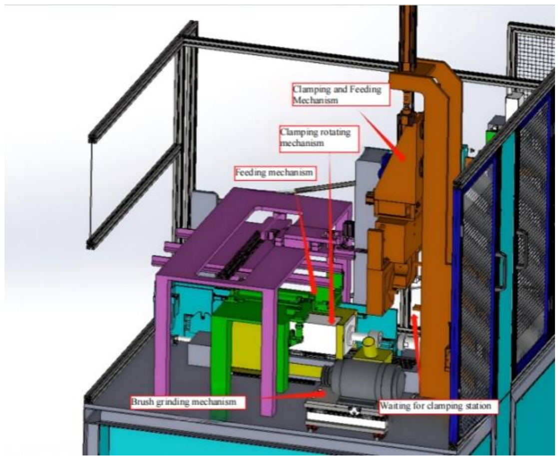

Figure 5 Schematic diagram of the designed production line structure

After the system is initiated, the feeding mechanism takes the lead in action, utilizing a dual-guide rod cylinder in conjunction with an electric cylinder to advance the piston ring on the feeding rack forward. Once the workpiece reaches the predetermined grasping point, the feeding gripper immediately intervenes to transfer it to the waiting clamping area. Immediately thereafter, the clamping feeding mechanism descends to pick up the workpiece and, in conjunction with the movable spindle box of the clamping rotating mechanism, completes the hydraulic locking of the workpiece. During the processing stage, the brushing mechanism performs surface treatment on the piston ring through a compound motion of longitudinal feed and lateral swing. Finally, the unloading grasping mechanism is responsible for removing the finished product, which is then organized by the ring sorting device and returned to the unloading rod, achieving full-process automation.

3 Design of the Brushing and Grinding Mechanism

This solution, based on the core function of the outer cylindrical grinding machine spindle rotation drive, replaces the original grinding wheel assembly with a dedicated brush wheel. It is equipped with a workpiece positioning system, cleaning liquid supply system, and protective recovery system, achieving automated and low-damage brushing of the piston ring's outer circumference, end face, and groove. This system is suitable for batch piston ring cleaning of carbon deposits and oil contamination.

① Brush selection and configuration: When selecting brush filaments for piston rings made of different materials, we need to conduct differentiated comparisons. For example, for gas rings, we need to choose nylon 612 filaments with a Shore hardness of

Table 1 Brush Wheel Assembly

Component Name	Specification parameters	Selection criteria
Brush material	Ring: nylon 612 brushed wire (Shore hardness 70-80); Uncoated ring: soft stainless steel brushed wire (wire diameter φ0.08-0.1mm)	The nylon bristles exhibit excellent flexibility to prevent coating scratches; the soft steel bristles effectively remove stubborn carbon deposits without damaging the metal substrate.
Brush wheel structure	Integrated hub with detachable brush ring, featuring an inner diameter compatible with grinding machine spindle (e.g., φ80mm/φ100mm)	Facilitates rapid replacement of worn brushes, reducing maintenance costs
Brush length and density	Brush length 15-20 mm, density ≥80 roots/cm²	Ensure full contact with the piston ring surface while preventing excessive bending of the brush hairs to avoid incomplete cleaning.
special accessories	Ring groove brush head: Customized elongated strip brush (width 2-5mm), mounted on the grinding machine tool holder via an extension rod	To meet the deep cleaning requirements of piston ring grooves, replace manual pointed brush operations

70-80 to prevent damage to the coating during brushing. For piston rings without a coating, we use soft stainless steel filaments with a diameter of 0.08-0.1mm, which can maximize the removal of carbon deposits without damaging the coating. The length of the brush filaments is set to 10-20mm, and the density is controlled to be above 100 filaments per cm to ensure sufficient contact.

② Speed and process control: Adjust the spindle speed via inverter from the original grinding machine's 1000–3000 r/min to 200–500 r/min. In terms of process, air ring cleaning is performed at low speed (200–300 r/min), while stubborn stain removal is carried out at medium speed (300–500 r/min) to prevent workpiece deformation.

③ Improvement of fixture: Replace the traditional three-jaw chuck with a pneumatic collet combined with polyurethane soft jaws, with clamping force controlled at 0.1–0.3 MPa, which protects the workpiece surface while ensuring a coaxiality accuracy of ≤0.02 mm.

4 Conclusion

The core practical significance of this design lies in promoting intelligent upgrading of the engine component industry, thereby enhancing enterprise competitiveness. By establishing a new intelligent production line featuring multi-station material loading, full-process coordination, and energy-saving optimization, this project successfully achieves an automated and continuous production model for piston ring external brushing. This innovation not only improves production efficiency and machining .

accuracy but also significantly reduces labor and energy costs. It effectively addresses the issues of low efficiency and poor precision inherent in traditional single-station equipment, fundamentally eliminating the potential risk of engine failures caused by burr detachment, and well aligns with current demands for efficient and high-precision manufacturing.

Fund Projects: The Foundation of Liaoning Provincial Key Laboratory of Energy Storage and Utilization (CNNK202522).

References

[1] Li Kaishun. Development and Research of High-Speed Response Piston Ring CNC Lathe [D]. Master's Thesis, Yangzhou University, April 2005.

[2] Zhu Youhui. China piston ring industry status and development prospects [J]. Internal Combustion Engine Parts, 2001(1):89-94.

[3] Liu Mingdeng, Lu Qijian. Application of linear motor and DSP high-speed motion controller[J]. China Mechanical Engineering, 1999(10):56-61.

[4] Lu Qijian. Direct Drive Technology for Linear Motors[J]. Mechanical and Electronic, 2001(4):71-77.

[5] Lai Guoting, Wu Yuhou, Fu Dawei. Linear motor speed/acceleration feedforward control based on PMAC[J]. Control Engineering, 2002(3):111-114.

[6] Li Jizhong, Li Kaishun, Wu Yingxue et al. Research on Piston Ring Machining and New NC Lathe Scheme[J]. Electromechanical Product Development and Innovation, 2004(3):93-94.

Publisher: Viser Technology Pte. Ltd.

URL: www.viserdata.com

Add.: 195 Pearl's Hill Terrace, #02-41,

Singapore 168976

ISSN 2661-443X